Journal of Biomolecular NMR, **25:** 113–123, 2003.
KLUWER/ESCOM
© 2003 *Kluwer Academic Publishers. Printed in the Netherlands.*

NMR of bicelles: orientation and mosaic spread of the liquid-crystal director under sample rotation

Giorgia Zandomeneghi, Marco Tomaselli, Philip T. F. Williamson & Beat H. Meier*
Physical Chemistry, ETH Zurich, ETH-Hönggerberg, CH-8093 Zurich, Switzerland

Received 21 August 2002; Accepted 31 October 2002

Key words: bicelle, liquid-crystal, NMR, order parameter, variable-angle spinning

Abstract

Model-membrane systems composed of liquid-crystalline bicellar phases can be uniaxially oriented with respect to a magnetic field, thereby facilitating structural and dynamics studies of membrane-associated proteins. Here we quantitatively characterize a method that allows the manipulation of the direction of this uniaxial orientation. Bicelles formed from DMPC/DHPC are examined by ^{31}P NMR under variable-angle sample-spinning (VAS) conditions, confirming that the orientation of the liquid-crystalline director can be influenced by sample spinning. The director is perpendicular to the rotation axis when Θ (the angle between the sample-spinning axis and the magnetic field direction) is smaller than the magic angle, and is parallel to the rotation axis when Θ is larger than the magic angle. The new ^{31}P NMR VAS data presented are considerably more sensitive to the orientation of the bicelle than earlier ^{2}H studies and the analysis of the sideband pattern allows the determination of the orientation of the liquid-crystal director and its variation over the sample, i.e., the mosaic spread. Under VAS, the mosaic spread is small if Θ deviates significantly from the magic angle but becomes very large at the magic angle.

Introduction

Bicelles self-organize from a mixture of long- and short-chain phospholipids in water (Sanders and Schwonek, 1992; Sanders et al., 1994; Sanders and Landis, 1995; Vold and Prosser, 1996). Liquid-crystalline phases consisting of bicelles are formed if the total lipid concentration, the ratio of the two phospholipids, the temperature and the pH of the solution are in the appropriate range. In this phase the phospholipids are assumed to form bilayered disks with a planar bilayer of long-chain DMPC phospholipids surrounded by a rim of shorter-chain DHPC (Vold and Prosser, 1996). Recently, this model has been questioned and a model where DMPC constitutes an highly dynamic perforated bilayer and DHPC forms the rims surrounding the holes has been proposed (Gaemers and Bax, 2001; Nieh et al., 2001, 2002). For the interpretation of our data, both models are equivalent but in our graphical representations we use the standard model. In a magnetic field, $\mathbf{B}_0$, the liquid-crystalline phase becomes oriented with the director perpendicular to $\mathbf{B}_0$. This particular director orientation is a consequence of the negative anisotropy of the diamagnetic susceptibility tensor, $\Delta\chi$.

Bicelles are attractive as model membranes for the study of phospholipid-associated proteins (Sanders and Landis, 1995; Glover et al., 2001; Howard and Opella, 1996; Losonczi and Prestegard, 1998; Struppe et al. 1998). Well-oriented liquid-crystalline phases can represent a viable alternative to mechanically oriented bilayers on glass plates (Marassi et al., 1999; Moll and Cross, 1990). In experiments with bicellar systems, in particular for the study of membrane-bound proteins, it is interesting to manipulate the orientation of the liquid-crystalline director e.g. by sample-spinning techniques. For spinning frequencies larger than a critical frequency, which depends on the strength of $\mathbf{B}_0$, $\Delta\chi$ and the Leslie viscosity coefficient, the director orients such that the magnetic energy averaged over a rotor cycle,

*To whom correspondence should be addressed. E-mail: beme@ethz.ch

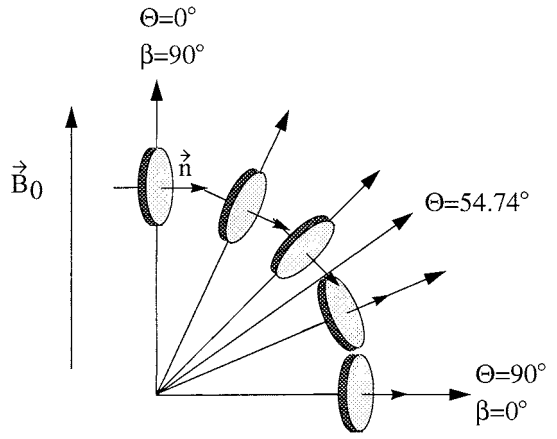

Figure 1. Energetically most favorable orientation of the bicelle director with respect to the rotor axis at different angles Θ between the rotor axis and $\mathbf{B}_0$.

$$E_{mag}(\Theta, \beta) = -\frac{\Delta\chi}{3\mu_0} B_0^2 \cdot P_2(\cos\Theta) \cdot P_2(\cos\beta), \tag{1}$$

is minimized (Courtieu et al., 1982, 1994). Here, Θ is the angle between the magnetic field and the spinning axis $\boldsymbol{\nu}_r$ and β is the angle between the bicelle director and $\boldsymbol{\nu}_r$. The vacuum permeability is denoted by μ_0 and the second-order Legendre polynomial by $P_2(\cos\theta) = (3\cos^2\theta - 1)/2$.

Two regimes of orientational behavior can be distinguished, as illustrated in Figure 1. In the range $0° \leq \Theta \leq \Theta_m$ (where Θ_m is the magic angle, $\Theta_m \approx 54.7°$) the energy is minimized when the bicelle director is perpendicular to the rotation axis ($\beta = 90°$) (Tian et al., 1999); for the range $\Theta_m < \Theta \leq 90°$, the minimum corresponds to the parallel orientation ($\beta = 0°$) (Zandomeneghi et al., 2001). At the magic angle, the magnetic energy is independent of the director orientation and the bicelles are predicted from Equation 1 to be randomly oriented.

Our earlier work focused on the residual quadrupolar splitting of the deuterium resonance of the solvent water (Zandomeneghi et al., 2001). The dependence of the orientation of the director on the angle Θ as expressed by Equation 1, was experimentally confirmed for spinning frequencies between 400 and 800 Hz. For angles $\Theta_m < \Theta \leq 90°$, especially at higher spinning frequencies (above 900 Hz), an additional phase was detected and assigned to an orientation with $\beta = 90°$. Furthermore, it was shown that the director can be aligned with $\mathbf{B}_0$ by switched-angle spinning (SAS) techniques. This orientation is spectroscopically attractive because it results in a single resonance line per site and therefore improves the spectral resolution (Howard and Opella, 1996; Prosser et al., 1998).

A number of different SAS experiments can be envisioned to correlate spectra at different orientations or to distinguish between scalar and dipolar couplings. In a companion paper (Zandomeneghi et al., 2003) we describe the realization of SAS experiments applied to bicelles containing phospholipid-associated peptides.

Here we report a ^{31}P NMR study of the effect of sample spinning on the magnetic orientation of bicellar systems. We show that ^{31}P spectroscopy can be used to describe not only the most likely orientation of the director but also the mosaic spread. This allows us also to characterize the additional phase that is sometimes observed in particular at higher spinning frequency or for angles Θ close to the magic angle.

The ^{31}P spectra of oriented bicelles

The spin interaction observed in the ^{1}H-decoupled ^{31}P NMR spectrum is the anisotropic chemical-shielding interaction. The frequency ω in the NMR spectrum is determined by σ, the *zz* component of the cartesian CSA tensor in the laboratory frame, $\underline{\sigma}^L$, according to

$$\omega = -\sigma\omega_0 = -(\underline{\sigma}^L)_{zz}\omega_0, \tag{2}$$

where ω_0 is the Larmor frequency.

Chemical-shielding-anisotropy (CSA) tensors will be characterized by the isotropic value $\bar{\sigma}$, the anisotropy δ, and the asymmetry-parameter η which are defined in terms of the elements of the cartesian matrix representation as $\bar{\sigma} = (\sigma_{xx} + \sigma_{yy} + \sigma_{zz})/3$, $\delta = \sigma_{zz} - \bar{\sigma}$ and $\eta = (\sigma_{xx} - \sigma_{yy})/\delta$.* In the principal axis system, the CSA tensor has the representation:

$$\begin{aligned}\underline{\sigma}^C &= \begin{bmatrix} \sigma_{xx} & 0 & 0 \\ 0 & \sigma_{yy} & 0 \\ 0 & 0 & \sigma_{zz} \end{bmatrix} \\ &= \bar{\sigma}\begin{bmatrix} 1 & 0 & 0 \\ 0 & 1 & 0 \\ 0 & 0 & 1 \end{bmatrix} + \frac{\delta^C}{2}\begin{bmatrix} -1 & 0 & 0 \\ 0 & -1 & 0 \\ 0 & 0 & 2 \end{bmatrix} \\ &\quad + \frac{1}{2}\delta^C\eta^C\begin{bmatrix} 1 & 0 & 0 \\ 0 & -1 & 0 \\ 0 & 0 & 0 \end{bmatrix}. \end{aligned} \tag{3}$$

*The three principal values of the space tensor are ordered according to the convention: $|\sigma_{zz} - \bar{\sigma}| \geq |\sigma_{yy} - \bar{\sigma}| \geq |\sigma_{xx} - \bar{\sigma}|$

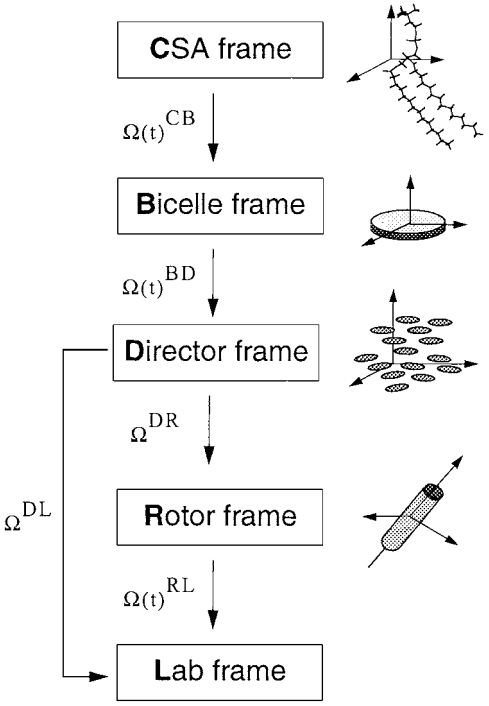

Figure 2. Summary of coordinate frames employed to calculate the ^{31}P spectra.

To calculate the spectrum, the CSA tensor in the laboratory frame must be known. This can be obtained through the series of reference frame transformations outlined in Figure 2. Each transformation is described by a set of three Euler angles, denoted by $\Omega = (\alpha, \beta, \gamma)$.

The first transformation is from the principal axis system (CSA frame) located at the phosphorous nucleus to the bicelle frame, with its z-axis normal to the DMPC plane in the bicelle. The Euler angles for this transformation $\Omega(t)^{CB}$ are stochastically time-dependent due to internal rotations, overall molecular rotation and molecular diffusion (Kohler and Klein, 1977; Seelig, 1978; Dufourc et al., 1992). Significantly different behavior between DMPC and DHPC is expected for the molecular diffusion. In both models for bicelles DMPC diffuses in a plane, leaving $\underline{\sigma}$ invariant. DHPC, in contrast, diffuses over a curved surface which could be modelled as half of a torus (Vold and Prosser, 1996; Picard et al., 1999).

The second transformation leads to the director frame, with its z-axis along the director of the particular liquid-crystalline domain. The corresponding set of Euler angles $\Omega(t)^{BD}$ is again stochastically time-dependent due to dynamic deviations of an individual bicelle normal from the direction of the director of the liquid crystalline phase. In the time average, these angles vanish: $\langle\Omega(t)^{BD}\rangle = (0, 0, 0)$.

If the correlation time of the motions creating the time dependence of $\Omega(t)^{CB}$ and $\Omega(t)^{BD}$ is short compared to the NMR timescale, defined by $(\delta^C\omega_0)^{-1}$ and in the order of 100 μs, the NMR spectrum from each domain is described by an averaged tensor $\underline{\sigma}^D$, characterized by $\bar{\sigma}$ and δ^D. Due to the axial symmetry, we expect $\eta^D = 0$ and the unique axis of $\underline{\sigma}^D$ to lie along the liquid-crystalline director. This behavior is indeed found in our experiments (vide infra) for both DHPC and DMPC. Due to the geometrical differences in the motion of DMPC and DHPC, the anisotropy, δ^D, is quite different for the two components (Vold and Prosser, 1996).

The anisotropy in the director frame is related to the anisotropy in the principal axis system by

$$\delta^D = S_{Bic} \cdot \delta^C \left[\left\langle \frac{(3\cos^2\beta^{CB} - 1)}{2} \right\rangle + \frac{\eta^C}{2} \langle \sin^2\beta^{CB} \cos 2\alpha^{CB} \rangle \right]. \quad (4)$$

The brackets $\langle\rangle$ denote time-averages and $S_{Bic} = \langle 3\cos^2\beta^{BD} - 1\rangle/2$ is the order parameter (Saupe, 1964) associated with the bicelle motion around the director.

In the following step, the CSA tensor must be transformed from the director frame (of each domain) to the rotor frame, a coordinate system fixed to the rotor (the sample container) with its z-axis parallel to the rotation axis.

This transformation is described by the Euler rotation Ω^{DR}. Due to symmetry, only two Euler angles are needed, i.e., $\Omega^{DR} = (0, \beta, \gamma)$. In general, β and γ do not assume a single value but are characterized by probabilities $p(< \beta)$ and $p(\gamma)$ because the sample can consist of several domains, each of them containing a large number of bicelles. Each domain can have a different director orientation with respect to the rotor frame. In particular, γ will be randomly distributed, because the energy in Equation 1 depends only on β. In general, the angle β will also be distributed and we will call this distribution the mosaic spread. We assume, that the director of each domain remains constant on the NMR timescale and that bicelles do not diffuse from one domain to the other. Therefore, this transformation does not involve time averaging and leaves $\bar{\sigma}$, δ and η invariant.

The final step, from the rotor frame to the laboratory frame, is described by the periodically time-dependent transformation, $\Omega^{RL}(t) = (-2\pi\nu_r t, -\Theta, 0)$, where ν_r is the rotor frequency and Θ the angle between the rotor axis and the magnetic field.

Transforming the bicelle-frame CSA tensor to the laboratory frame leads to the following expression for $\sigma = (\underline{\sigma}^L)_{zz}$:

$$\sigma(\nu_r, \Theta, \beta, \gamma, t) = \bar{\sigma} + \delta^D \cdot P_2(\cos\beta) \cdot P_2(\cos\Theta) + \Psi(\nu_r, \Theta, \beta, \gamma, t). \quad (5)$$

The time-dependent terms due to sample rotation are collected in the following relation:

$$\Psi(\nu_r, \Theta, \beta, \gamma, t) = C_1(\beta, \Theta)\cos(2\pi\nu_r t + \gamma) + C_2(\beta, \Theta)\cos(4\pi\nu_r t + 2\gamma), \quad (6)$$

with

$$C_1(\beta, \Theta) = -\tfrac{3}{4}\delta^D \sin(2\beta)\sin(2\Theta) \quad (7)$$

and

$$C_2(\beta, \Theta) = \tfrac{3}{4}\delta^D \sin(\beta)^2 \sin(\Theta)^2. \quad (8)$$

For a well-defined value of the angle β (corresponding to a vanishing mosaic spread of the liquid-crystal director) the spectrum consists of two families of sharp resonance lines for DHPC and DMPC, each consisting of a central line flanked by spinning sidebands separated by integer multiples of ν_r. The centerband resonance position depends on the angles Θ and β as follows:

$$\omega_{CB}(\beta, \Theta) = -(\bar{\sigma} + \delta^D \cdot P_2(\cos\beta) \cdot P_2(\cos\Theta))\omega_0. \quad (9)$$

For a uniform distribution of the angle γ, $p(\gamma) = 1/2\pi$, all spinning sidebands are positive absorption lines with the intensity of the Nth sideband described by (Mehring, 1983)

$$I_N(\beta, \Theta) = \left| \frac{1}{2\pi} \int_0^{2\pi} \exp\left[i\left(-N\phi - \frac{\omega_0 C_1(\beta, \Theta)}{2\pi\nu_r}\sin(\phi) - \frac{\omega_0 C_2(\beta, \Theta)}{4\pi\nu_r}\sin(2\phi)\right)\right] d\phi \right|^2. \quad (10)$$

We characterize the mosaic spread by a Gaussian distribution of the angle β centered at $\bar{\beta}$ and with standard deviation μ,

$$p(\beta) = \frac{1}{\mu\sqrt{2\pi}} \cdot \exp\left(-\frac{1}{2}\left(\frac{\beta - \bar{\beta}}{\mu} \right)^2 \right). \quad (11)$$

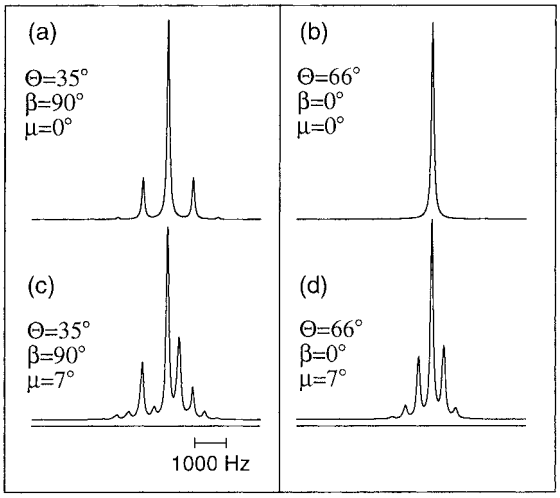

Figure 3. Simulation of DMPC ^{31}P NMR sideband spectra for (a) $\Theta = 35°$ and $\bar{\beta} = 90°$ and $\mu = 0°$, (b) $\Theta = 66°$ and $\bar{\beta} = 0°$ and $\mu = 0°$, (c) $\Theta = 35°$ and $\bar{\beta} = 90°$ and $\mu = 7°$, and (d) $\Theta = 66°$ and $\bar{\beta} = 0°$ and $\mu = 7°$. The highest peak is the centerband. In (a) only even order sidebands are observed, (b) shows no sidebands. The mosaic spread leads to the presence of even and odd order sidebands in (c) as well as in (d). For the anisotropy the value $\delta^D_{DMPC} = -22.0$ ppm was used. Isotropic chemical shielding was $\bar{\sigma} = 0$ ppm. Note that $\omega_{CB}(90°, 35°) \approx \omega_{CB}(0°, 66°)$.

For a non-vanishing mosaic spread, the centerand sidebands will be heterogeneously broadened into a tensor pattern. The NMR spectrum is calculated according to

$$S(\Theta, \omega) = \frac{1}{2} \cdot \int_0^{\pi} \left(\sum_{N=-\infty}^{\infty} I_N(\beta, \Theta) \cdot \delta_D(\omega - \omega_{CB}(\beta, \Theta) - 2\pi N\nu_r) \right) p(\beta) \cdot \sin\beta \, d\beta, \quad (12)$$

where δ_D denotes the Dirac delta function. Finally, a Lorentzian line broadening can be added.

The resulting spinning-sideband patterns in the NMR spectrum are sensitive to $\bar{\beta}$ and to the mosaic spread μ. We note that a perfectly oriented sample with $\bar{\beta} = 90°$ would give only even order sidebands while a perfectly oriented sample with $\bar{\beta} = 0°$ would give no sidebands at all, as shown in Figures 3a and 3b, respectively. In Figures 3c and 3d, the corresponding calculated spectra for a mosaic spread of $\mu = 7°$ are given. They illustrate the strong sensitivity of the sideband intensities to μ.

Static spectra can be described with the same formalism (Figure 2). The Euler angles $\Omega^{DL} = (0, \beta, \gamma)$ define the transformation from the director frame to

the laboratory frame. Again we use the Gaussian distribution of Equation 11 with $\bar{\beta} = 90°$ and a random distribution for γ.

Materials and methods

Sample preparation

Fifty milligrams of lipids (1,2-Dihexanoyl-*sn*-glycero-3-phosphocholine (DHPC) and 1,2-Ditetradecanoyl-*sn*-glycero-3-phosphocholine (DMPC), [DMPC]/[DHPC] = 3.5) were mixed with 150 µl of H_2O. The following procedure was repeated 3 times: vortexing (2 min), heating to 40 °C (20 min), vortexing (2 min), cooling to 0 °C (20 min). Lipids were purchased from Avanti Polar Lipids (Alabaster, AL). All experiments were performed with freshly prepared samples.

NMR experiments

^{31}P NMR experiments were performed on a home-built spectrometer (Hediger et al., 1997) at a magnetic field of 7.00 Tesla (^{31}P resonance frequency of $\omega_0/2\pi = -120.66$ MHz), with a Chemagnetics MAS probehead, using 4 mm rotors (internal diameter is 2.5 mm). The probehead was modified in order to enlarge the range of accessible angles to 25°–90°. We used 90° pulses of 3–4.5 µs. The spectral width was 20 kHz and the ^{1}H decoupling strength between 24 and 39 kHz. For each spectrum between 1000 and 4000 transients were acquired with a recycle time of 3 s. All measurements were done at 37 °C. The rotation angles Θ have been measured by an inclinometer with an experimental uncertainty of 2.5°. The magic angle was calibrated on the ^{79}Br signal of a spinning sample of polycrystalline KBr.

Simulations and calculations

Spectra have been processed with MATNMR.* The lineshape simulations were calculated in C++, using the GAMMA spin-simulation environment (Smith et al., 1994). The powder averaging was performed according to Cheng (Cheng et al., 1973) with either 538 or 1154 powder orientations per spectrum. The least square fitting was performed with the program MINUIT.** The errors here reported are the ones obtained by MINUIT and represent one standard deviation.

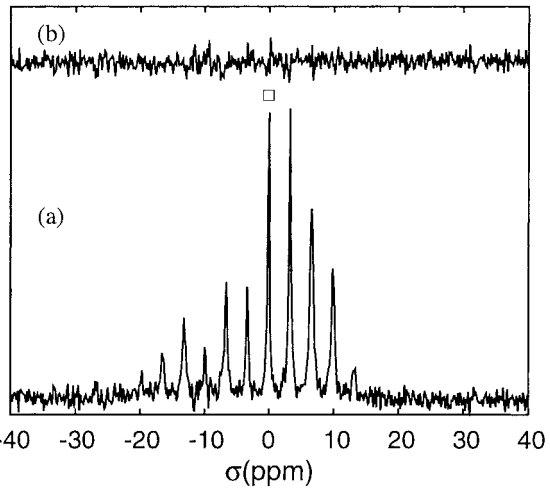

Figure 4. (a) Experimental ^{31}P NMR spectrum obtained under magic-angle spinning at $\nu_r = 400$ Hz and (b) difference between the experimental and the fit described in the text. The spectrum reported has been measured 14 hours after spinning was started. The frequency scale is given in units of the chemical shielding, as defined in Equation 2.

Results and discussion

MAS spectra

The experimental ^{31}P magic-angle spinning (MAS) spectrum of a bicellar phase of DMPC/DHPC is shown in Figure 4a. It consists of a single centerband (marked by a square) and the corresponding sideband family, indicating that the isotropic shieldings of DMPC ($\bar{\sigma}_{DMPC}$) and DHPC ($\bar{\sigma}_{DHPC}$) are identical within our spectral resolution. In the following, we will reference all spectra to this isotropic shielding at the given temperature, setting $\bar{\sigma}_{DMPC} = \bar{\sigma}_{DHPC} = \bar{\sigma} = 0$ ppm. Referencing to 85% H_3PO_4 leads, at T = 310 K, to $\bar{\sigma} \approx 0.84$ ppm.

At the magic angle, $\Theta_m \approx 54.7°$, the magnetic energy does not depend on Θ (Equation 1) and an isotropic distribution of the director orientation is expected. We will refer to such an isotropic distribution as a powder distribution. Note that powder distribution means that the director of different liquid-crystalline domains (each containing a large number of bicelles) is randomly oriented. The individual bicelles within one domain are still well-aligned with the director in this domain. The domains size is considerably larger

*MATNMR is a toolbox for processing NMR/EPR data under MATLAB and can be downloaded freely at http://www.nmr.ethz.ch/matnmr

**MINUIT, Cern Program Library Entry D506.

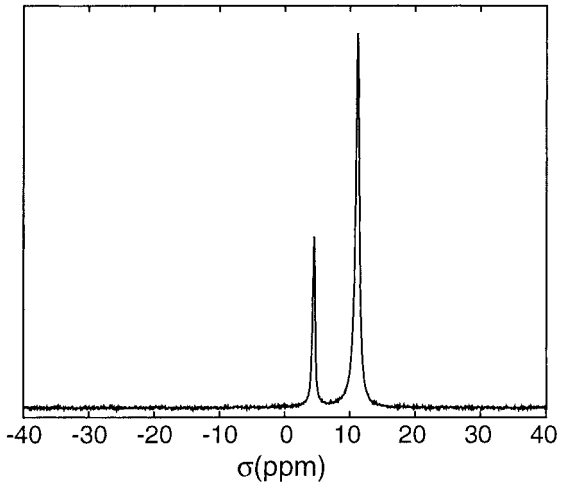

Figure 5. ^{31}P NMR spectrum of a static sample.

than the free mean path of the solvent water molecules during the duration of the NMR experiment (milliseconds), otherwise the ^{2}H splittings that have been observed (Zandomeneghi et al., 2001) would be absent. The statistic of the momentary misalignment of the bicelles with the director is described by the order parameter S_{Bic}.

The experimental sideband intensities in the ^{31}P spectrum of Figure 4a, obtained after spinning a sample at 400 Hz for 14 hours, are well described by a powder distribution of the director. Figure 4b shows the difference between the experimental data and a fit by a powder distribution for both phospholipids with the fitted anisotropies $\delta^{D}_{DMPC} = -21.7 \pm 0.6$ ppm and $\delta^{D}_{DHPC} = -7.9 \pm 0.5$ ppm. For shorter spinning times the director showed some preferred ordering, oriented perpendicular to the rotation axis.

Static samples

In Figure 5 the ^{31}P NMR spectrum of a static bicellar sample is reported. The spectrum consists of two sharp lines with resonance positions (relative to isotropic DHPC) of 11.25 ppm (DMPC) and 4.53 ppm (DHPC). The ratio of the peak integrals is, within experimental error, equal to the concentration ratio q = [DMPC]/[DHPC] = 3.5. It is well established (Sanders and Schwonek, 1992) that $\bar{\beta} = 90°$ for static samples. Therefore, the chemical shielding is

$$\sigma = \bar{\sigma} - \frac{\delta^{D}}{2}. \qquad (13)$$

The presence of one single sharp resonance line per compound corroborates that the chemical shielding tensors $\underline{\sigma}^{D}$ of both phospholipids are indeed axially symmetric. We have determined δ^{D}_{DMPC}, δ^{D}_{DHPC} (according to Equation 13) and q (from the peak integrals) in the temperature range from 304 K to 314 K. At 310 K, we found $\delta^{D}_{DMPC} = -23.0 \pm 0.4$ ppm, $\delta^{D}_{DHPC} = -9.2 \pm 0.4$ ppm and q = 3.4 ± 0.3. The error margins given above are the standard deviation from a series of measurements on 20 different samples and are indicative of a certain variability on details of the sample preparation, experimental temperature and sample history. Between 304 K to 314 K, the anisotropy of both components increases linearly with temperature, as described by linear coefficients $d\delta^{D}_{DMPC}/dT = -0.19$ ppm/K and $d\delta^{D}_{DHPC}/dT = -0.46$ ppm/K.

From a lineshape-analysis of the DHPC and DMPC signals, we can determine the mosaic spread to be $\mu = 4° \pm 2°$.

Variable-angle spinning

^{31}P NMR single pulse experiments were performed on bicelle samples spun at different angles Θ, using spinning frequencies in the range 400 Hz $\leq \nu_r \leq$ 800 Hz. A selection of spectra taken at 800 Hz is given in Figure 6. From the sharp features of the spectra, tentatively assigned to a well-ordered phase, the two spinning-frequency independent centerbands of DHPC and DMPC, as well as the associated spinning-sideband families have been identified. A rigorous justification for this assignment will be presented below. The center-band resonance frequency is plotted, as function of Θ in Figure 7. The solid lines in the figure correspond to a fit of these data using Equation 9 with $\beta = 90°$ for $\Theta < \Theta_m$ and $\beta = 0°$ for $\Theta > \Theta_m$. The fitted parameters are $\bar{\sigma}_{DMPC} = 0.0 \pm 0.2$ ppm, $\bar{\sigma}_{DHPC} = -0.1 \pm 0.1$ ppm, $\delta^{D}_{DMPC} = -22.7 \pm 0.8$ ppm and $\delta^{D}_{DHPC} = -9.3 \pm 0.4$ ppm. The anisotropies are found to be identical to the ones determined in the static experiment within the error margins, and the isotropic shieldings are found to be zero. The good agreement indicates that (i) the anisotropy δ^{D} for DHPC and DMPC (and therefore the order parameter of the liquid-crystalline phase) is not influenced by the spinning at frequencies used here. (ii) For angles Θ smaller than the magic angle, the director of the well-ordered majority phase is perpendicular to the spinning axis, while for angles larger than the

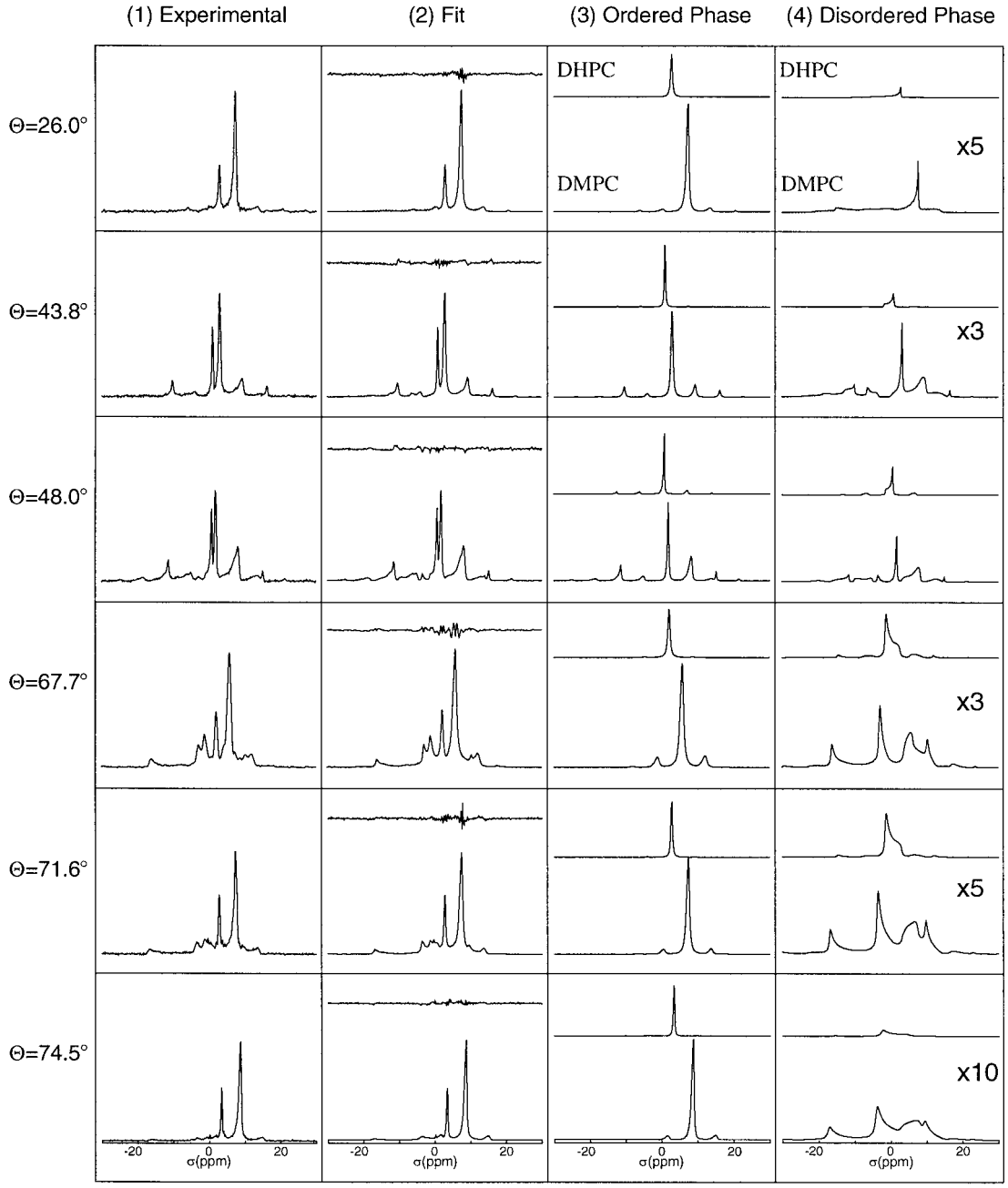

Figure 6. ^{31}P NMR spectra for different spinning angles Θ, obtained at a spinning frequency $\nu_r = 800$ Hz. Column 1: Experimental spectrum; column 2: Best fit (bottom) and difference between the experimental spectrum and the fit (top); column 3: Contribution to the fit from DMPC (bottom) and DHPC (top) in the oriented phase; column 4: Contribution to the fit from DMPC (bottom) and DHPC (top) in the powder phase. Where indicated, intensities are multiplied by 3, 5 or 10. After the start of the sample's spinning the evolution of the order was followed for about 12 h and the spectrum corresponding to the most ordered situation is reported here.

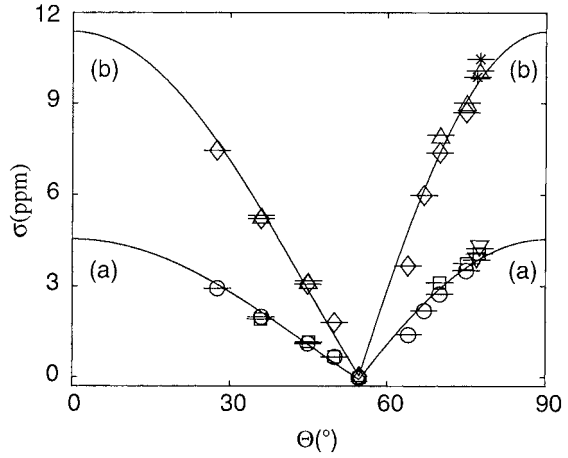

Figure 7. ^{31}P NMR resonance positions for bicelle samples spun around an axis tilted by angle Θ with respect to $\mathbf{B}_0$. Experimental points ($\Diamond$), (Δ) and ($*$) refer to DMPC peak, in experiments where $\nu_r = 800$ Hz, $\nu_r = 400$ Hz and $\nu_r = 550$, 600 Hz, respectively. Experimental points ($\bigcirc$), ($\Box$) and (∇) refer to DHPC peak, in experiments where $\nu_r = 800$ Hz, $\nu_r = 400$ Hz and $\nu_r = 550$, 600 Hz, respectively. Curve (a) describes $\sigma = -0.1 - P_2(\cos\bar{\beta}) \cdot 9.3 \cdot P(\cos\Theta)$, while Curve (b) represents $\sigma = 0.0 - P_2(\cos\bar{\beta}) \cdot 22.7 \cdot P_2(\cos\Theta)$. For $0° \leq \Theta < \Theta_m$, $P_2(\cos\bar{\beta}) = -0.5$ and for $\Theta_m < \Theta \leq 90°$, $P_2(\cos\bar{\beta}) = 1.0$. Angles Θ are given as evaluated by an inclinometer and the error bars in the chemical shieldings are smaller than the width of the symbols.

magic angle, the two vectors are parallel, as shown schematically in Figure 1.

For a more detailed evaluation of the experimental spectra, we have fitted each spectrum using Equation 12. The equation describes the spectrum for one compound, DHPC or DMPC, in a certain bicellar phase. We model our spectra as two different phases of bicelles, each one containing DMPC and DHPC and characterized by the stoichiometric ratio q, the anisotropy δ^D of DHPC and DMPC, the linewidth of the signals of DHPC and DMPC, and the mosaic spread μ. For the first phase, $\bar{\beta} = 90°$ for $\Theta < \Theta_m$ and $\bar{\beta} = 0°$ for $\Theta > \Theta_m$. For the second phase, $\bar{\beta} = 90°$ for all angles Θ (Bayle et al., 1988), in agreement with ^{2}H data for solvent water (Zandomeneghi et al., 2001). For $\nu_r < 850$ Hz, the mosaic spread for the minority phase was always found to be rather large ($\mu > 30°$) and it turned out, that spectra can be equally well described by a simpler model where the more disordered phase is represented by a random distribution of the director with respect to $\mathbf{B}_0$, $\mu \rightarrow \infty$. In the following, this randomly oriented phase is called the 'powder phase'. This model provides an excellent description of all experimental spectra with $\nu_r < 850$ Hz. Table 1 lists the parameters corresponding to the best fit of the experimental data of Figure 6 (column 1) and of further spectra not shown. Figure 6 shows the fitted spectra and the difference between experiment and fit in column 2. The four different contributions to the calculated spectra, namely the DHPC and DMPC spectra in the oriented and powder phase respectively, are shown in columns 3 and 4. Good agreement between fit and experiments is found. Free fitting parameters are those listed in Table 1, as well as a Lorentzian line broadening (different for DMPC and DHPC) and an overall intensity scaling. The spinning angle Θ has been set with an estimated precision of $\pm 2.5°$. However, it can also be used as a free fit parameter, despite the fact that δ^D and Θ have significant correlation. The deviation between manually determined and fitted value was consistently below $\pm 2.5°$.

It can be seen from column 3 of Figure 6 that the oriented phase leads, as expected, to a sharp sideband pattern for each component at all spinning angles Θ. The anisotropies δ^D_{DHPC} and δ^D_{DMPC} are independent of Θ (see Table 1). This finding fully corroborates the centerband-frequencies extracted directly from the spectra and plotted in Figure 7. The composition of the ordered phase, q, is always found to be around 3.5, as expected.

For angles away from the magic angle (e.g., $\Theta < 45°$ or $\Theta > 67°$) the mosaic spread of the bicellar phase is found to be around 7°. This is slightly higher than in static samples and similar to mechanically oriented lipid bilayers on glass plates where mosaic spreads of 4° (Glaubitz and Watts, 1998) for pure DMPC and 8° for a DMPC sample containing an integral membrane peptide have been reported (Moll and Cross, 1990).

Except at the magic angle, the powder phase is always the minority phase at the spinning speeds considered here. At angles close to 0° and 90°, its weight becomes negligibly small. When the proportion of the powder phase is high enough to obtain precise fit values, the anisotropies δ^D for both the phospholipids and the value of q are comparable with the ones found for the ordered phase and for the static samples. This finding indicates that the disordered phase is also composed of bicelles, with similar DMPC/DHPC composition, shape and dynamics.

The experimental values for μ and the relative weight of the two phases are somewhat influenced by the details of the sample history. For $\Theta < 45°$ or $\Theta > 67°$ the system assumes a constant degree of order after one hour, or even less, and this order starts

Table 1. δ^D values and ratio q = [DMPC]/[DHPC] for the oriented as well as for the powder phase, mosaic spread of the bicellar director's orientation, μ and amount of the powder phase determined in VAS experiments where the sample is spun at angles Θ with respect to $\mathbf{B}_0$ and at spinning frequency ν_r

Θ (°)	ν_r	Oriented phase				Powder phase			
	(Hz)	δ^D_{DMPC} (ppm)	δ^D_{DHPC} (ppm)	q	μ (°)	Powder phase (%)	δ^D_{DMPC} (ppm)	δ^D_{DHPC} (ppm)	q
26 (1)	800	−20.9(5)	−8.3(2)	3.4(1)	7.3 (3)	17(12)	−21.5(6)	−7.8(4)	8 (5)
36.1(2)	400	−21.7(2)	−8.0(1)	3.6(1)	6.8 (3)	7(4)	−20.4(4)	−7.1(8)	10 (7)
35.8(4)	800	−21.6(5)	−8.3(2)	3.6(2)	7.0 (4)	8(3)	−22.6(5)	−8.9(4)	8 (6)
43.9(1)	400	−23.1(1)	−8.8(1)	3.8(2)	5.9 (2)	20(4)	−21.5(2)	−7.3(2)	3.1(7)
43.8(2)	800	−21.8(4)	−7.7(1)	3.1(1)	8.5 (6)	36(7)	−23.4(4)	−6.5(5)	12 (7)
48.3(1)	430	−22.6(4)	−9.2(2)	3.4(3)	8.3 (5)	29(8)	−22.7(8)	−10.2(8)	2.3(5)
48.0(1)	800	−23.5(4)	−9.8(4)	3.4(4)	19 (2)	50(14)	−20.6(4)	−8.2(4)	3.8(7)
61.5(2)	800	−23.9(5)	−9.3(2)	3.4(2)	11.6 (4)	43(4)	−21.2(4)	−7.8(4)	3.4(4)
67.7(4)	800	−21.5(5)	−8.1(2)	3.7(2)	8.9 (4)	42(4)	−21.7(5)	−9.3(4)	3.4(4)
71.6(2)	400	−22.8(2)	−9.0(1)	4.0(2)	7.8 (2)	18(3)	−21.3(3)	−6.2(2)	5 (3)
71.6(5)	800	−21.8(5)	−8.4(2)	3.3(1)	7.3 (3)	42(3)	−21.1(5)	−8.4(5)	3.7(5)
74.6(2)	400	−22.9(1)	−9.8(1)	3.6(1)	6.05(8)	19(3)	−29.0(2)	−12.4(3)	2.8(8)
74.5(4)	800	−22.6(3)	−9.1(1)	3.7(1)	8.1 (1)	23(2)	−20.7(4)	−12.4(3)	10 (8)
78.5(3)	550	−22.8(1)	−9.0(1)	3.7(1)	7.8 (1)	18(2)	−19.8(3)	− 7.2(8)	13 (6)
79.2(4)	400	−22.3(2)	−8.8(1)	3.1(1)	6.6 (3)	3(3)	−26 (5)	−13 (6)	15 (7)
79.8(8)	600	−23.6(4)	−9.6(2)	3.4(2)	7.7 (3)	10(3)	−20 (5)	−13 (6)	15 (13)

to deteriorate only after several hours. For example an experiment performed at $\Theta = 26°$, $\nu_r = 800$ Hz showed the greatest order ($\mu = 7.3 \pm 0.3°$) after 1–2 h spinning. After 10 hours the order was reduced to $\mu = 10.6° \pm 0.6°$. The contribution of the powder phase is around 10% for both spectra and does not show a tendency to increase with time. For Θ closer to the magic angle Θ_m the phases are less stable; it takes a longer time to reach the most ordered state and the order is lost more quickly. For $\Theta = 61.5°$ the greatest order ($\mu = 11.6° \pm 0.4°$) is reached after 10 h spinning. Three hours later, the order had decreased to $\mu = 22° \pm 1°$. The resonance position of the central lines in both of the phases does not change with time, indicating that δ^D and $\bar{\beta}$ are not affected by prolonged spinning. All values reported in Table 1 and Figure 6 correspond to the state with the lowest μ.

At higher spinning frequencies (above 850 Hz), a change in the phase behavior is encountered. We have accelerated a sample, spun at $\Theta = 76.5°$, from $\nu_r = 410$ Hz to $\nu_r = 1840$ Hz (Figure 8). At the lower spinning frequency the sample behaved as described above, with an oriented phase at $\bar{\beta} = 0°$ with $\mu = 6.6° \pm 0.2°$, $\delta^D_{DMPC} = -22.6° \pm 0.2$ ppm, $\delta^D_{DHPC} = -9.1 \pm 0.2$ ppm and a randomly oriented phase with $23 \pm 3\%$ abundance (Figure 8a). After spinning 12 hours at $\nu_r = 1840$ Hz, the spectrum of Figure 8c was

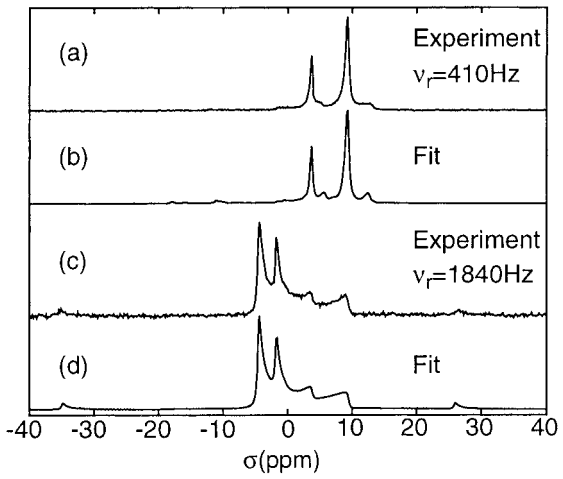

Figure 8. (a) ^{31}P NMR experimental spectrum at $\Theta = 76.5°$ with $\nu_r = 410$ Hz; (b) best fit; (c) experimental spectrum at $\nu_r = 1840$ Hz; (d) best fit. Note that the spinning-sideband pattern in spectrum (a) is not perfectly reproduced by the fit in (b), due to experimental instability in spinning rate which broadens the sidebands.

recorded. This spectrum contains two oriented phases: one phase with $63 \pm 25\%$ abundance and $\bar{\beta} = 90°$ with $\delta^{D}_{DMPC} = -21.6 \pm 0.1$ ppm, $\delta^{D}_{DHPC} = -8.7 \pm 0.1$ ppm, $q = 2.8 \pm 0.2$ and $\mu = 21° \pm 4°$ and another phase with $\beta = 0°$, $\delta^{D}_{DMPC} = -22.7 \pm 0.3$ ppm, $\delta^{D}_{DHPC} = -9.2 \pm 0.3$ ppm, $q = 3 \pm 1$ and $\mu = 28° \pm 7°$. This indicates that, for higher spinning rates, a new oriented bicellar phase appears with the director perpendicular to the spinning axis. This observation is in accordance with ^{2}H NMR experiments at $\Theta = 79°$ and $\nu_r = 920$ Hz which also indicate that an oriented phase with $\bar{\beta} = 90°$ appears for faster spinning (Zandomeneghi et al., 2001). It should however be noted, that the mosaic spread of both oriented phases is significantly higher than observed for slower spinning.

It is possible that the same, not fully understood forces that stabilize the $\bar{\beta} = 90°$ phase for fast spinning are responsible for the transient order observed when the sample is spun at the magic angle.

Conclusions

Under variable-angle sample-spinning at frequencies below about 800 Hz, liquid-crystalline bicelle phases behave like 'ordinary' nematic liquid crystals with $\Delta\chi < 0$: the director of the dominant phase is perpendicular to the rotation axis when the sample is spun at angles smaller than the magic angle and it orients parallel to the rotation axis when the angles are bigger. When the rotation angle is not near the magic angle, the phase is well ordered with a mosaic spread μ of around 7°. As the rotation angle approaches the magic angle, a second phase of increasing abundance is noted. This phase is much less ordered and can be well described by a powder distribution (no orientational order with respect to the magnetic field). At higher spinning frequencies two partially ordered phases have been detected at $\Theta = 76.6°$. They have their directors parallel and perpendicular to the spinning axis, respectively.

Our findings show that bicelles in rotating samples are a promising medium for the investigation of membrane-bound peptides and proteins. The mosaic spread is comparable to the one in static samples or to the one of bilayers deposited on glass plates. The conditions can be optimized such that the disordered phase does not contribute significantly to the spectrum. Notably, for angles close to $\Theta = 90°$ a highly ordered state can be created and maintained. From this initial state, a switched-angle spinning experiment can prepare bicelles with the director parallel to the applied field. In addition, we propose an experiment where magic-angle-spinning spectra are obtained using SAS techniques with the sample rotating at the magic angle, or close to it, only for the short time required to pulse and collect the NMR signal (see companion paper, Zandomeneghi et al., 2003).

Acknowledgements

We are grateful to Matthias Ernst, Megan Spence, Urban Meier and Andreas Hunkeler for helpful discussion and for experimental assistance.

References

Bayle, J.P., Perez, F. and Courtieu, J. (1988) *Liq. Cryst.*, **3**, 753–758.
Cheng, V.B., Suzukawa, H.H. and Wolfsberg, M. (1973) *J. Chem. Phys.*, **59**, 3992–3999.
Courtieu, J., Alderman, D.W., Grant, D.M. and Bayles, J.P. (1982) *J. Chem. Phys.*, **77**, 723–730.
Courtieu, J., Bayle, J.P. and Fung, B.M. (1994) *Prog. Nucl. Magn. Reson. Spectrosc.*, **26**, 141–169.
Dufourc, E.J., Mayer, C., Stohrer, J., Althoff, G. and Kothe, G. (1992) *Biophys. J.*, **61**, 42–57.
Gaemers, S. and Bax, A. (2001) *J. Am. Chem. Soc.*, **123**, 12343–12352.
Glaubitz, C. and Watts, A. (1998) *J. Magn. Reson.*, **130**, 305–316.
Glover, K.J., Whiles, J.A., Wood, M.J., Melacini, G., Komives, E.A. and Vold, R.R. (2001) *Biochemistry*, **40**, 13137–13142.
Hediger, S., Signer, P., Tomaselli, M., Ernst, R.R. and Meier, B.H. (1997) *J. Magn. Reson.*, **125**, 291–301.
Howard, K.P. and Opella, S.J. (1996) *J. Magn. Reson. Ser.*, **B112**, 91–94.
Kohler, S.J. and Klein, M.P. (1977) *Biochemistry*, **16**, 519–526.
Losonczi, J.A. and Prestegard, J.H. (1998) *Biochemistry*, **37**, 706–716.
Marassi, F.M., Opella, S.J., Juvvadi, P. and Merrifield, R.B. (1999) *Biophys. J.*, **77**, 3152–3155.
Mehring, M. (1983) *Principles of High Resolution NMR in Solids*, Springer-Verlag, Berlin.
Moll, F. and Cross, T.A. (1990) *Biophys. J.*, **57**, 351–362.
Nieh, M.P., Glinka, C.J., Krueger, S., Prosser, R.S. and Katsaras, J. (2001) *Langmuir*, **17**, 2629–2638.
Nieh, M.P., Glinka, C.J., Krueger, S., Prosser, R.S. and Katsaras, J. (2002) *Biophys. J.*, **82**, 2487–2498.
Picard, F., Paquet, M.J., Levesque, J., Belanger, A. and Auger, M. (1999) *Biophys. J.*, **77**, 888–902.
Prosser, R.S., Hwang, J.S. and Vold, R.R. (1998) *Biophys. J.*, **74**, 2405–2418.
Sanders, C.R. and Landis, G.C. (1995) *Biochemistry*, **34**, 4030–4040.
Sanders, C.R. and Schwonek, J.P. (1992) *Biochemistry*, **31**, 8898–8905.
Sanders, C.R., Hare, B.J., Howard, K.P. and Prestegard, J.H. (1994) *Prog. Nucl. Magn. Reson. Spectrosc.*, **26**, 421–444.
Saupe, A. (1964) *Z. Naturforsch.*, **19a**, 161–171.
Seelig, J. (1978) *Biochim. Biophys. Acta*, **515**, 105–140.

Smith, S.A., Levante, T.O., Meier, B.H. and Ernst, R.R. (1994) *J. Magn. Reson. Ser.*, **A106**, 75–105.

Struppe, J., Komives, E.A., Taylor, S.S. and Vold, R.R. (1998) *Biochemistry*, **37**, 15523–15527.

Tian, F., Losonczi, J.A., Fischer, M.W.F. and Prestegard, J.H. (1999) *J. Biomol. NMR*, **15**, 145–150.

Vold, R.R. and Prosser, R.S. (1996) *J. Magn. Reson. Ser.*, **B113**, 267–271.

Zandomeneghi, G., Tomaselli, M., Van Beek, J.D. and Meier, B.H. (2001) *J. Am. Chem. Soc.*, **123**, 910–913.

Zandomeneghi, G., Williams, P.T.F., Hunkeler, A. and Meier, B.H. (2003) *J. Biomol. NMR*, **25**, 125–132.